Materials Advances

ROYAL SOCIETY OF CHEMISTRY

PAPER

View Article Online
View Journal | View Issue

Cite this: *Mater. Adv.*, 2023, 4, 2379

Synthesis of extended covalently bound porphyrins on the Au(111) surface

José J. Ortiz-Garcia * and Rebecca C. Quardokus

Received 20th February 2023,
Accepted 2nd April 2023

DOI: 10.1039/d3ma00081h

rsc.li/materials-advances

Solution deposition of a 5,10,15,20-tetrakis-(4-bromophenyl)-porphyrin (TBrPP) and dichloromethane (DCM) on the Au(111) surface produces self-assembled islands with a non-random orientation that is directed by the gold herringbone reconstruction of Au(111). Annealing to 230 °C caused approximately 1/3 of the surface adsorbed porphyrins to interact with the underlying gold adatom leading to Au-TBrPP intermediates. The position of the TBrPP molecules corresponded with the soliton walls of the gold herringbone reconstruction. Annealing to 300 °C caused dehalogenated C–C coupling between TBrPP and DCM as well as the metalation of TBrPP. This reaction created polymeric chains of TBrPP with DCM linkers. The molecular chains are flexible and can be easily manipulated using a scanning tunneling microscope (STM) tip.

1 Introduction

Porphyrin and porphyrin-like molecules have been of interest due to their role in biological and chemical processes such as gas transport and light harvesting photosynthetic roles.[1–3] To date, porphyrins have been used to serve a large variety of purposes in biomedicine,[4,5] sensing,[5,6] formation of extended covalent networks,[7–11] and catalysis[3,12–14] due to their versatile and tunable nature. The efficiency of these molecules in biological systems has thus inspired researchers to look towards biology for ideas of new technologies.[3] Over the years, the potential of these molecules for more applications such as molecular photovoltaics[15,16] and memory storage devices[17–19] has expanded their use and interest in these molecules.

On surfaces, porphyrins are well-established as molecular building blocks due to their inherent functionality, molecular structure, and structural stability.[20] When deposited on a metallic surface, porphyrins will self-assemble leading to the formation of well-ordered porphyrin islands. The self-assembling nature of these molecules has allowed researchers to probe their robustness as well as their electronic properties using a scanning tunneling microscope (STM). Furthermore, it has been seen that these molecules could indeed be coupled and metallated on a surface using heat-assisted processes such as annealing[21–23] and tip-induced bond formation,[24–26] leading to increased interest in porphyrins for the fabrication of nanoscale structures such as nanomeshes and covalent organic frameworks (COFs).

The role of the underlying substrate, such as Au(111), can have an influence on the self-assembly and electronic properties of the adsorbate.[20,27–33] Observations of the formation of Au–porphyrin intermediates *via* solution-based deposition methods of a porphyrin self-assembled monolayer on the Au(111) surface reveal similar features upon surface modification, such as electrochemical reactions. Kim *et al.* discovered that the interaction between metalloporphyrins and the underlying Au(111) substrate results in synergistic effects on the catalytic activity of the oxygen evolution reaction.[34] Rana *et al.* conducted research on a double decker molecule that contains phthalocyanine and observed that, on the Au(111) surface, the Au atoms bind to the double decker molecules, resulting in a significant decrease in the molecules' mobility when compared to studies conducted on a highly oriented pyrolytic graphite surface.[35] Moreover, recent studies have demonstrated that the Au(111) herringbone affects the electronic states of a TFPP porphyrin, leading to the formation of two equivalent conformations of the molecule with shifted electronic states.[36] Therefore, investigating the interplay between the underlying Au(111) substrate and its role in the electronic structure and chemical properties of porphyrins is crucial for further understanding. Here, the Au(111) herringbone plays a role in the self-assembly and on-surface metalation of a pulse-deposited solution of TBrPP. The formation of covalently linked porphyrins and dichloromethane (DCM) *via* dehalogenative C–C coupling (Ullman-like coupling) was observed. Furthermore, molecular manipulation experiments demonstrated the flexibility of the covalent-organic frameworks and carbon–carbon covalent coupling.

2 Materials and methods

Experiments were performed using a low-temperature ultra-high vacuum scanning tunneling microscope (LT-UHV-STM, Scienta Omicron) system operated at 77 K. The STM tip was a

Department of Chemistry, University of Connecticut, Storrs, CT, USA.
E-mail: rebecca.quardokus@uconn.edu

mechanically clipped 0.25 mm Pt80/Ir20 wire (NanoScience Instruments). All images were obtained in a constant current mode. The substrate was Au(111) on mica (Phasis) and was prepared using cycles of argon-ion sputtering and annealing. The STM images of the Au(111) substrate after sputtering and annealing confirmed that the substrate was clean. The sample was prepared at room temperature by depositing a 1.01 mM solution of 5,10,15,20-tetrakis-(4-bromo-phenyl)porphyrin (TBrPP) dissolved in DCM using the pulsed-solenoid valve in a vacuum chamber on the clean Au(111) surface.

TBrPP was imaged as deposited followed by step-wise annealing to monitor the Ulman-like coupling of the porphyrin and DCM. The electronic structures of TBrPP and Au-TBrPP were calculated using density functional theory (DFT) calculations. The structure was optimized using the B3LYP functional and the 6-311+G(d) basis set.[37,38] The harmonic vibrational frequency analysis confirmed that the structure was at a local minimum without any imaginary frequencies. All calculations were done using Gaussian 16 Rev. A.03.[39] STM images were simulated using the Tersoff and Hamann approximation[40,41] as performed previously.[36,42,43] Molecular manipulation experiments were performed to determine the flexibility of the COFs and corroborate that the molecules were covalently coupled.

3 Results and discussion

The pulsed deposition of TBrPP leads to the formation of self-assembled porphyrin islands. It is observed that the orientation of the porphyrin islands is influenced by the herringbone reconstruction of the underlying Au(111) substrate, highlighted by the yellow lines, as shown in Fig. 1. This type of surface templating has been observed in other adsorbate/substrate systems such as small molecules and porphyrin-like molecules.[44–48]

The stepwise annealing of TBrPP was performed to study the effects of annealing on the porphyrin self-assembled monolayer as well as to remove an excess DCM solvent from the sample. Annealing the molecule up to 128 °C led to changes in the conformational structure of the molecule as well as a change in the adsorption site due to thermally induced diffusion. The TBrPP porphyrin changed from a square porphyrin with four lobes as shown in Fig. 1 to a dimmer porphyrin.

Sequential annealing up to 232 °C further leads to changes in the conformational structure of the porphyrins in which there are four bright lobes of the porphyrins surrounded by four small lobes probably due to the Br atoms as shown in Fig. 2a. These TBrPP molecules appear with a dim central depression. Interestingly enough, bright protrusions at the center of the porphyrins are also observed in Fig. 2a which appear to light up with no apparent order. Fig. 2b shows the zoomed out image of the area imaged in Fig. 2a. It was noticed that the underlying herringbone, outlined by the yellow dashed lines in Fig. 2b, could explain the appearance of these porphyrins. The reconstruction pattern here is seen to line up with the porphyrins which appear with bright protrusions due to them sitting atop the gold herringbone. This evidences that not only does the gold herringbone play a role in shifting the molecule's electronic states but can also lead to gold metallated porphyrins (Au-TBrPP) with this being the predetermining step for porphyrin metalation. Edmondson *et al.* reported similar structures *via* STM while studying a 2*H*-tetraphenylporphyrin (2*H*-TPP)

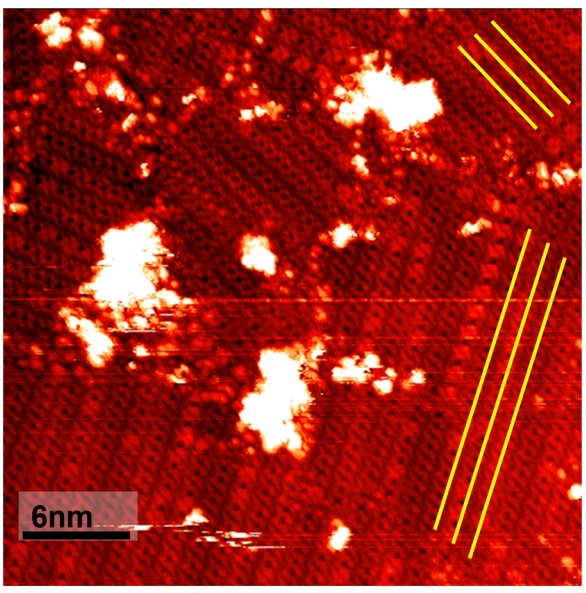

Fig. 1 Occupied electronic states of TBrPP porphyrins on Au(111). Porphyrins self-assemble following the gold herringbone pattern as outlined by the yellow lines. The 33 nm × 33 nm image was taken at a bias voltage of −1.0 V and an $I_{Setpoint}$ of 10 pA.

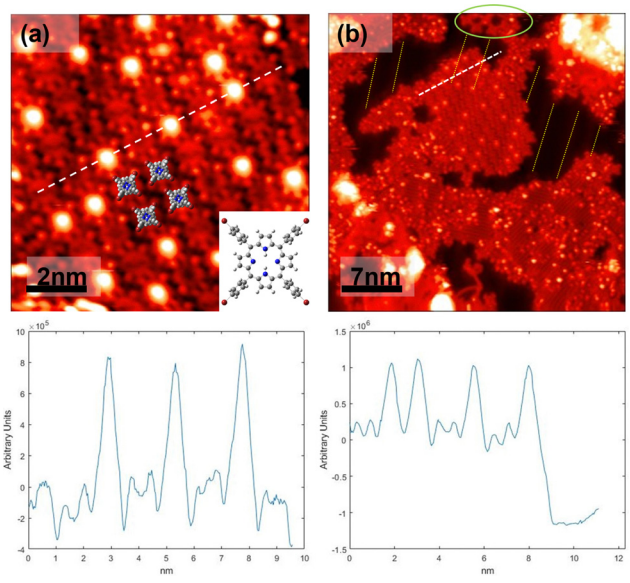

Fig. 2 (a) 35 × 35 nm STM image of the TBrPP sample taken at a bias voltage of −1.5 V and an $I_{Setpoint}$ of 10 pA. The yellow dashed lines outline the underlying herringbone reconstruction. The green circle shows the formation of a COF *via* Ulman-like coupling. (b) 10 × 10 nm STM image of the free-base and gold-influenced TBrPP taken at a bias voltage of −1.5 V and an $I_{Setpoint}$ of 10 pA. The gold atom appears as a bright central protrusion in the TBrPP molecule. The white dashed lines outline the cross-sectional Z-profiling of the STM images.

molecule and the effects of annealing. Their research revealed close-packed monolayers of 2*H*-TPP at −193.15 °C, which appeared with a central depression. Upon annealing to 167 ± 50 °C, they found the evidence of metalation through XPS and scanning tunneling spectroscopy.[49] Additionally, the evidence of Ullman-like coupling was seen at this annealing step and was circled in green showing the formation of a small COF, composed of TBrPP. The white dashed line in Fig. 2a is a cross-section of both TBrPP porphyrins with bright protrusions and depressions showing the difference in their respective height profiles. The bright protrusion leads to a higher apparent height due to the influence of the underlying gold atoms on the TBrPP electronic states.

Annealing to 300.6 °C leads to the further formation of low-dimensional materials *via* Ulman-type coupling. The TBrPP molecules are seen in Fig. 3a forming the molecular wires of varying sizes. In addition, the formation of some strained molecular frameworks is seen in Fig. 3a, made clearer with a zoomed-in inset. This is hypothesized to be due to the result of the TBrPP molecule Ullman-like coupling to other TBrPP molecules through the DCM solvent leading to the formation of some interesting arrays of porphyrin–solvent 2D materials. Annealing to 300.6 °C allows for the TBrPP porphyrins to break free from molecule–molecule intermolecular forces and the substrate–molecule intermolecular forces as evidenced by the change of their adsorption sites and the orientation on the surface as shown in Fig. 3b. Furthermore, it is observed that some of these TBrPP molecules still maintained their central bright protrusions even after annealing to 300.6 °C is also evidenced in Fig. 3b leading to the hypothesis that these are fully metallated TBrPP (Au-TBrPP). Further annealing to 348 °C leads to the formation of longer Ulman-like coupled porphyrin 2D materials as well as the increased diffusion of the porphyrin molecules leading to the streaks in some of the images. Simulated STM images taken using the Tersoff and Hamann approximations corroborate the experimental STM images. The simulated TBrPP HOMO through HOMO-3, as shown in Fig. 4a,

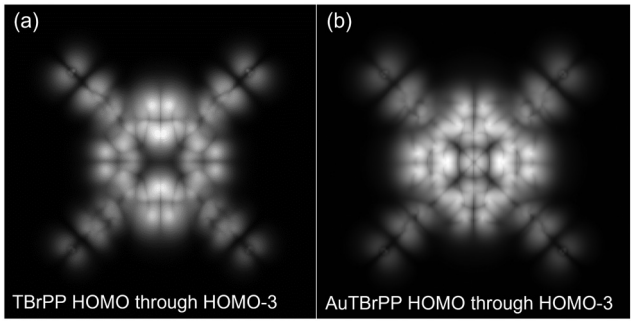

Fig. 4 (a) STM simulated image of the HOMO through the HOMO-3 of the TBrPP molecule. (b) STM simulated image of the HOMO through the HOMO-3 of the Au-TBrPP molecule. Both images were optimized using Gaussian 16 followed by frequency calculations. STM images were simulated using the resulting electronic structure from the Gaussian 16 software using the Tersoff and Hamann approximation.

can be seen to be in good agreement with the experimental STM images shown in Fig. 2a. Additionally, simulated STM images of Au-TBrPP, as shown in Fig. 4b, are also in good agreement with the experimental images seen in Fig. 3b with the bright protrusion at the center.

To show that the porphyrins had undergone C–C coupling *via* Ulman-like coupling molecular manipulation experiments were performed in which the STM tip was brought into close proximity to a covalently bound porphyrin group. Following this, the current set point was increased to ≈8 nA leading to the STM tip picking up the porphyrin group and dragging it as shown in Fig. 5a. This resulted in the COF of porphyrins being moved towards another COF of porphyrins. Additionally, this procedure was repeated to move the porphyrins back towards their original position as shown in Fig. 5b leading to Fig. 5c. The stability of the porphyrin groups and their ability to remain intact through the molecular manipulation experiment corroborate the hypothesis that the porphyrins are indeed covalently bound. If porphyrin groups were stabilized *via* molecule–molecule interactions, then it would be expected that only one

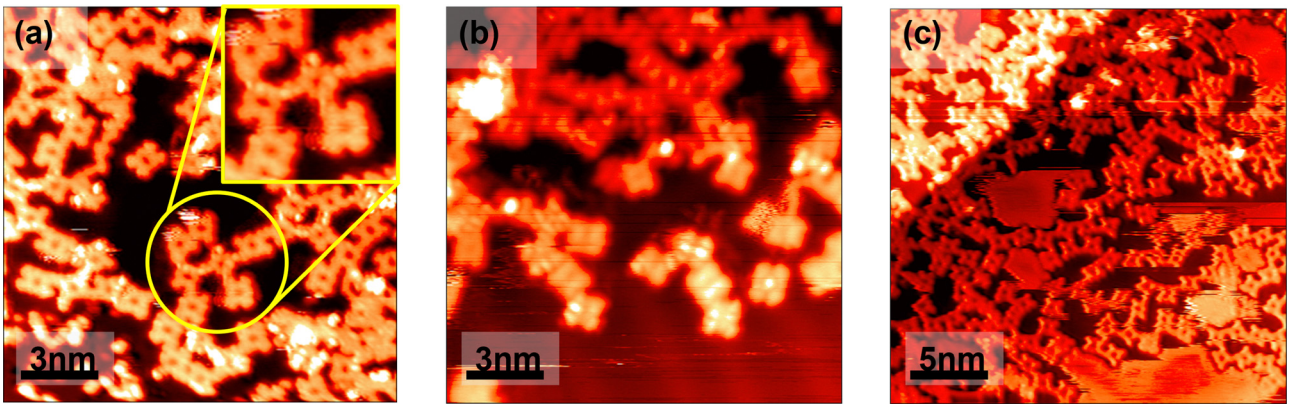

Fig. 3 (a) Formation of the Ullman-like coupled COF of porphyrin–porphyrin molecules as well as porphyrin–solvent–porphyrin molecules leading to a strained like COF at a temperature of 300.6 °C. The inset is a zoomed-in image of the strained COF showing the porphyrin–solvent–porphyrin C–C coupling. (b) TBrPP molecules with bright central protrusions, Au-TBrPP, observed to also participate in Ullman-like coupling. (c) Annealing to 348 °C lead to the formation of longer Ullman-like coupled porphyrin molecular wires and COFs. The STM imaging conditions are as follows: (a) $I_{Setpoint}$ = 10 pA and a bias voltage of 2.0 V, (b) $I_{Setpoint}$ = 14 pA and a bias voltage of 2.0 V, and (c) $I_{Setpoint}$ = 1.0 nA and a bias voltage of 0.5 V.

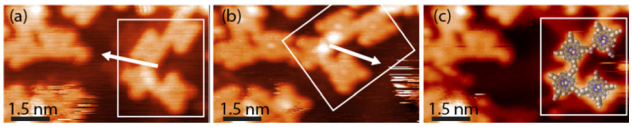

Fig. 5 (a–c) Molecular manipulation of TBrPP porphyrins using the STM tip. Ullman-coupled porphyrins were moved back and forth showing the structural stability afforded to the low-dimensional frameworks through the C–C bond formation. (c) A TBrPP model is inseted to show the relative position and geometry of the porphyrin molecules. (a–c) STM images were obtained using an $I_{Setpoint}$ = 20 pA and a bias voltage of −2.0 V.

porphyrin molecule would be dragged from the group breaking the molecule–molecule interactions.

4 Conclusions

In conclusion, TBrPP dissolved in DCM was pulse deposited onto the Au(111) surface *via* the pulse deposition valve.[50] TBrPP molecules were observed to tightly pack on the surface following the Au(111) herringbone reconstruction pattern. The fine interplay between the molecule–molecule and the molecule–substrate interactions that govern the self-assembly of the TBrPP molecules on the surface was elucidated. Gentle annealing of the TBrPP molecules up to 232 °C led to an increase in the interaction between the Au(111) atoms on the herringbone lines and the nitrogens of the TBrPP porphyrins leading to changes in the electronic states of approximately 33% of the TBrPP molecules. It is hypothesized that these TBrPP porphyrins are not yet metallated but their interaction with the underlying Au(111) atoms is significant and is a transition step towards the full metalation of TBrPP. Additionally, at 232 °C, Ullman-like coupling was observed to begin occurring, in agreement with work performed by Grill *et al.*[51,52] Annealing at a temperature of 300.3 °C led to the formation of low-dimensional materials *via* Ulman-like coupling. Interestingly enough, annealing at this temperature provided enough thermal energy for the DCM solvent to interact with the TBrPP porphyrins leading to the formation of strained molecular frameworks. At this temperature, there was also evidence of fully metallated Au-TBrPP molecules that had moved away from the herringbone reconstruction lines through thermal diffusion. Furthermore, the possibility of metalation through resistive heating was evidenced. Annealing to 348 °C leads to the formation of longer Ulman-like coupled molecular wires on the surface as well as more diffusion of the molecules on the surface. Molecular manipulation experiments were performed to corroborate the fact that the molecular wires were indeed C–C coupled to each other. The fact that they remained intact through the molecular manipulation experiment confirms that they were indeed Ullman coupled and not molecule–molecule stabilized.

This study shows the possibility of using solution based deposition methods to lead to the formation of Ullman-like coupling reactions. Deposition methods such as the PDV method are interesting due to the fact that they allow the solution phase to be compatible with vacuum science. Additionally, they allow for the deposition of solution stabilized molecules as they do not change them *via* thermal deposition leading to interesting assemblies on a surface as well as the possibility of the formation of low dimensional materials on a surface.

Author contributions

José Ortiz-Garcia contributed to the collection and evaluation of experimental data, data curation, DFT calculations, theoretical STM calculations, formal analysis, and the writing of the manuscript. Rebecca C. Quardokus was involved in conceptualization, data curation, formal analysis, supervision, and the writing of the manuscript.

Conflicts of interest

There are no conflicts to declare.

References

1 C. J. Kingsbury and M. O. Senge, *Coord. Chem. Rev.*, 2021, **431**, 213760.
2 S. Pina-Oviedo, C. Ortiz-Hidalgo and A. G. Ayala, *Arch. Pathol. Lab. Med.*, 2017, **141**, 445–462.
3 A. H. Proppe, Y. C. Li, A. Aspuru-Guzik, C. P. Berlinguette, C. J. Chang, R. Cogdell, A. G. Doyle, J. Flick, N. M. Gabor, R. van Grondelle, S. Hammes-Schiffer, S. A. Jaffer, S. O. Kelley, M. Leclerc, K. Leo, T. E. Mallouk, P. Narang, G. S. Schlau-Cohen, G. D. Scholes, A. Vojvodic, V. W. W. Yam, J. Y. Yang and E. H. Sargent, *Nat. Rev. Mater.*, 2020, **5**, 828–846.
4 M. Imran, M. Ramzan, A. K. Qureshi, M. A. Khan and M. Tariq, *Biosensors*, 2018, **8**, 1–17.
5 N. Tsolekile, S. Nelana and O. S. Oluwafemi, *Molecules*, 2019, **24**, 1–15.
6 K. Norvaiša, M. Kielmann and M. O. Senge, *ChemBioChem*, 2020, **21**, 1793–1807.
7 S. Y. Ding, J. Gao, Q. Wang, Y. Zhang, W. G. Song, C. Y. Su and W. Wang, *J. Am. Chem. Soc.*, 2011, **133**, 19816–19822.
8 S. Lin, C. S. Diercks, Y.-B. Zhang, N. Kornienko, E. M. Nichols, Y. Zhao, A. R. Paris, D. Kim, P. Yang, O. M. Yaghi and C. J. Chang, *Science*, 2015, **349**, 1208–1213.
9 C. Chen, T. Joshi, H. Li, A. D. Chavez, Z. Pedramrazi, P. N. Liu, H. Li, W. R. Dichtel, J. L. Bredas and M. F. Crommie, *ACS Nano*, 2018, **12**, 385–391.
10 C. J. Judd, D. V. Kondratuk, H. L. Anderson and A. Saywell, *Sci. Rep.*, 2019, **9**, 1–8.
11 S. Bhunia, K. A. Deo and A. K. Gaharwar, *Adv. Funct. Mater.*, 2020, **30**, 2002046.
12 X. Wang, Z. F. Cai, D. Wang and L. J. Wan, *J. Am. Chem. Soc.*, 2019, **141**, 7665–7669.
13 X. Zhang, M. Cibian, A. Call, K. Yamauchi and K. Sakai, *ACS Catal.*, 2019, **9**, 11263–11273.
14 A. Call, M. Cibian, K. Yamamoto, T. Nakazono, K. Yamauchi and K. Sakai, *ACS Catal.*, 2019, **9**, 4867–4874.
15 M. Urbani, M. Grätzel, M. K. Nazeeruddin and T. Torres, *Chem. Rev.*, 2014, **114**, 12330–12396.

16 G. Yang, Y. Tang, X. Li, H. Agren and Y. Xie, *ACS Appl. Mater. Interfaces*, 2017, **9**, 36875–36885.
17 P. Liljeroth, J. Repp and G. Meyer, *Science*, 2007, **317**, 1203–1206.
18 W. Auwärter, K. Seufert, F. Bischoff, D. Ecija, S. Vijayaraghavan, S. Joshi, F. Klappenberger, N. Samudrala and J. V. Barth, *Nat. Nanotechnol.*, 2012, **7**, 41–46.
19 Z. Feng, S. Velari, C. Dri, A. Goldoni, M. Peressi and G. Comelli, *J. Phys. Chem. C*, 2020, **124**, 11376–11382.
20 W. Auwärter, D. Écija, F. Klappenberger and J. V. Barth, *Nat. Chem.*, 2015, **7**, 105–120.
21 F. Klappenberger, A. Weber-Bargioni, W. Auwärter, M. Marschall, A. Schiffrin and J. V. Barth, *J. Chem. Phys.*, 2008, **129**, 214702.
22 T. Kumagai, F. Hanke, S. Gawinkowski, J. Sharp, K. Kotsis, J. Waluk, M. Persson and L. Grill, *Phys. Rev. Lett.*, 2013, **111**, 246101.
23 B. Cirera, B. D. L. Torre, D. Moreno, M. Ondrácek, R. Zboril, R. Miranda, P. Jelínek and D. Écija, *Chem. Mater.*, 2019, **31**, 3248–3256.
24 A. Sperl, J. Kröger and R. Berndt, *Angew. Chem., Int. Ed.*, 2011, **50**, 5294–5297.
25 W. Auwärter, K. Seufert, F. Bischoff, D. Ecija, S. Vijayaraghavan, S. Joshi, F. Klappenberger, N. Samudrala and J. V. Barth, *Nat. Nanotechnol.*, 2012, **7**, 41–46.
26 L. Smykalla, P. Shukrynau, C. Mende, T. Rüffer, H. Lang and M. Hietschold, *Surf. Sci.*, 2014, **628**, 92–97.
27 T. Yokoyama, S. Yokoyama, T. Kamikado and S. Mashiko, *J. Chem. Phys.*, 2001, **115**, 3814–3818.
28 S. Müllegger, W. Schöfberger, M. Rashidi, L. M. Reith and R. Koch, *J. Am. Chem. Soc.*, 2009, **131**, 17740–17741.
29 S. Müllegger, M. Rashidi, T. Lengauer, E. Rauls, W. G. Schmidt, G. Knör, W. Schöfberger and R. Koch, *Phys. Rev. B: Condens. Matter Mater. Phys.*, 2011, **83**, 165416.
30 F. Hanke and J. Björk, *Phys. Rev. B: Condens. Matter Mater. Phys.*, 2013, **87**, 235422.
31 Y. Gurdal, J. Hutter and M. Iannuzzi, *J. Phys. Chem. C*, 2017, **121**, 11416–11427.
32 Y. Kim, Y. Kim and J. Y. Park, *Langmuir*, 2020, **36**, 3792–3797.
33 J. J. Ortiz-Garcia and R. C. Quardokus, *J. Vac. Sci. Technol., A*, 2023, **41**, 030801.
34 Y. Kim, Y. Jeong, Y. Kim and J. Y. Park, *Adv. Mater. Interfaces*, 2021, **8**, 2100873.
35 S. Rana, J. Jiang, K. V. Korpany, U. Mazur and K. Hipps, *J. Phys. Chem. C*, 2021, **125**, 1421–1431.
36 M. Wolf, J. J. Ortiz-Garcia, M. J. Guberman-Pfeffer, J. A. Gascón and R. C. Quardokus, *RSC Adv.*, 2022, **12**, 1361–1365.
37 A. D. Becke, *J. Phys. Chem.*, 1993, **98**, 5648–5652.
38 P. J. Stephens, F. J. Devlin, C. F. Chabalowski and M. J. Frisch, *J. Phys. Chem.*, 1994, **98**, 11623–11627.
39 M. J. Frisch, G. W. Trucks, H. B. Schlegel, G. E. Scuseria, M. A. Robb, J. R. Cheeseman, G. Scalmani, V. Barone, G. A. Petersson, H. Nakatsuji, X. Li, M. Caricato, A. V. Marenich, J. Bloino, B. G. Janesko, R. Gomperts, B. Mennucci, H. P. Hratchian, J. V. Ortiz, A. F. Izmaylov, J. L. Sonnenberg, D. Williams-Young, F. Ding, F. Lipparini, F. Egidi, J. Goings, B. Peng, A. Petrone, T. Henderson, D. Ranasinghe, V. G. Zakrzewski, J. Gao, N. Rega, G. Zheng, W. Liang, M. Hada, M. Ehara, K. Toyota, R. Fukuda, J. Hasegawa, M. Ishida, T. Nakajima, Y. Honda, O. Kitao, H. Nakai, T. Vreven, K. Throssell, J. A. Montgomery Jr., J. E. Peralta, F. Ogliaro, M. J. Bearpark, J. J. Heyd, E. N. Brothers, K. N. Kudin, V. N. Staroverov, T. A. Keith, R. Kobayashi, J. Normand, K. Raghavachari, A. P. Rendell, J. C. Burant, S. S. Iyengar, J. Tomasi, M. Cossi, J. M. Millam, M. Klene, C. Adamo, R. Cammi, J. W. Ochterski, R. L. Martin, K. Morokuma, O. Farkas, J. B. Foresman and D. J. Fox, *Gaussian 16 Revision A.03*, Gaussian Inc., Wallingford CT, 2016.
40 J. Tersoff and D. R. Hamann, *Phys. Rev. Lett.*, 1983, **50**, 25.
41 J. Tersoff and D. R. Hamann, *Phys. Rev. B: Condens. Matter Mater. Phys.*, 1985, **31**, 805–813.
42 R. C. Quardokus, Y. Lu, N. A. Wasio, C. S. Lent, F. Justaud, C. Lapinte and S. A. Kandel, *J. Am. Chem. Soc.*, 2012, **134**, 1710–1714.
43 R. C. Quardokus, N. A. Wasio, J. A. Christie, K. W. Henderson, R. P. Forrest, C. S. Lent, S. A. Corcelli and S. A. Kandel, *Chem. Commun.*, 2014, **50**, 10229–10232.
44 M. Corso, L. Fernández, F. Schiller and J. E. Ortega, *ACS Nano*, 2010, **4**, 1603–1611.
45 Q. Fan, J. Dai, T. Wang, J. Kuttner, G. Hilt, J. M. Gottfried and J. Zhu, *ACS Nano*, 2016, **10**, 3747–3754.
46 B. Cirera, O. Trukhina, J. Björk, G. Bottari, J. Rodríguez-Fernández, A. Martin-Jimenez, M. K. Islyaikin, R. Otero, J. M. Gallego, R. Miranda, T. Torres and D. Ecija, *J. Am. Chem. Soc.*, 2017, **139**, 14129–14136.
47 B. D. B. Cortés, N. Schmidt, M. Enache and M. Stöhr, *J. Phys. Chem. C*, 2019, **123**, 19681–19687.
48 A. Trembulowicz, A. Sabik and M. Grodzicki, *Molecules*, 2021, **26**, 2393.
49 M. Edmondson, E. S. Frampton, C. J. Judd, N. R. Champness, R. G. Jones and A. Saywell, *Chem. Commun.*, 2022, **58**, 6247–6250.
50 M. Wolf, V. Hayes, C. R. Gerber, P. G. Quardokus, J. J. Ortiz-Garcia, C. Plummer and R. C. Quardokus, *J. Vac. Sci. Technol., A*, 2020, **38**, 022413.
51 L. Grill, M. Dyer, L. Lafferentz, M. Persson, M. V. Peters and S. Hecht, *Nat. Nanotechnol.*, 2007, **2**, 687–691.
52 L. Lafferentz, V. Eberhardt, C. Dri, C. Africh, G. Comelli, F. Esch, S. Hecht and L. Grill, *Nat. Chem.*, 2012, **4**, 215–220.